Eur. Phys. J. B **46**, 207–213 (2005)
DOI: 10.1140/epjb/e2005-00222-4

THE EUROPEAN PHYSICAL JOURNAL B

Effects of Coulomb interaction on charge transport in a silicon-based nanocluster array

K.I. Mazzitello[1], H.O. Mártin[1], and H.E. Roman[2,a]

[1] Departamento de Física, Facultad de Ciencias Exactas y Naturales, Universidad Nacional de Mar del Plata, Funes 3350, 7600 Mar del Plata, Argentina
[2] Dipartimento di Fisica, Università di Milano-Bicocca, Piazza della Scienza 3, 20126 Milano, Italy

Received 29 November 2004
Published online 19 July 2005 –

Abstract. The effects of Coulomb interaction on charge transport in a model of light emission from an array of silicon nanoclusters are studied by Monte Carlo simulations. The array is sandwiched between a p-type and an n-type doped silicon crystals and electrons and holes are driven into the array by an applied electric field. Radiative recombinations of electrons and holes take place near the center of the array producing the emission of red light, and the total emission power is approximately proportional to the current injected into the system. It is found that the carrier-carrier interaction plays a crucial role in charge transport. Specifically, the self-interaction of charges inside each nanocluster is found to be the dominant interaction term for the semiclassical Hamiltonian considered. In addition, it drastically limits the current in the device giving rise to a strong non-linear relation between current and density of free carriers in the doped silicon crystals.

PACS. 05.40.-a Fluctuation phenomena, random processes, noise, and Brownian motion – 05.60.-k Transport processes – 73.63.-b Electronic transport in nanoscale materials and structures

1 Introduction

An open problem in optoelectronic systems is to efficiently produce light from the injection of charges into a silicon based device (see, e.g. [1–8]). Recently, a prototype of a silicon nanocluster (NC) array has been introduced and studied theoretically [9]. The model consists of an assembly of silicon nanoclusters sandwiched between p- and n-type doped silicon crystals, which act as charge reservoirs of holes and electrons, respectively. The carriers are driven into the array by an applied electric field, producing red light when radiative recombinations take place. It is found that the efficiency for light emission is quite large, between about 2% and 0.5% for fields ranging from 100 to 500 kV/cm, respectively, at the temperature $T = 300$ K [9]. The light emission takes place near the center of the array, where nanoclusters having a diameter of about 3.6 nm are located, and the total emission power is approximately proportional to the total current injected into the system.

Due to the small size of the nanoclusters two distinct effects appear. One of them is quantum-confinement, which allows for visible light emission with rather large yield. For example, a silicon nanocluster of 3.6 nm diameter has a yield of about 1/3 (i.e., on average, one photon is produced for every three electron-hole recombinations [6]) and light emission occurs predominantly in the visible red. A second phenomenon is the presence of the Coulomb self-interaction between the additional charges brought inside a nanocluster. This interaction is not acting in ordinary crystal semiconductors because charge confinement does not take place in the bulk. Thus, one must necessarily deal with the Coulomb interaction in the study of charge transport in nanoclusters arrays.

The main purpose of the present work is to estimate, from a semi-classical point of view, the main effects of the Coulomb interaction on charge transport and total light emission power for the array of nanoclusters introduced in [9]. The present calculations are aimed to extend and complement the results discussed in [9], permitting us to draw more general conclusions on the role of Coulomb interactions in such silicon nanocluster arrays.

The paper is organized as follows. In Section 2 the model is briefly reviewed together with a discussion of the different approximations performed. The charge carriers dynamics is simulated by means of the Metropolis-Monte Carlo method, whose rules are summarized in Section 3. The numerical results are discussed in Section 4, where a simple analytical model is presented in the case of non interacting carriers. A summary and concluding remarks are given in Section 5.

[a] e-mail: eduardo.roman@mib.infn.it

2 Silicon nanocluster array

Realistic models of nanoclusters devices necessarily consist of several thousands of atomic or molecular units (see e.g. Fig. 1), for which first principles calculations of transport properties remain elusive. The less ambitious goal of using parametrized tight-binding Hamiltonians still remains prohibited. A promising approach to attack the transport problem of a many-nanocluster system is to resort to a semiclassical Hamiltonian (see Sect. 3) which can be solved in a very efficient fashion by Monte Carlo methods.

The spatial disposition of nanoclusters illustrated in the top panel of Figure 1 suggests us to consider the idealized one-dimensional array of nanoclusters shown in the lower panel of Figure 1, which is expected to capture the essential geometrical and carrier-carrier interaction aspects [9]. The electronic properties of the Si nanoclusters used in our calculations are summarized in Appendix A, where the relation between optical gap E and radius R of each nanocluster is given (see Eq. (6) below). The (indirect) optical gaps in the doped silicon crystals (boxes in Fig. 1) take their bulk value $E_{\rm Bulk} = 1.17$ eV.

In what follows, the index $1 \leq i \leq N$ indicates the ith NC, where R_i and E_i are its radius and optical gap, respectively (see Eq. (6)). Here, we have taken $N = 400$, $E_{1,N} = 1.25$ eV (i.e. $R_{1,400} = 80$ Å) and the central NC at $i = 200$ and 201 have $E_{200,201} = 1.8$ eV (i.e. $R_{200,201} = 18$ Å), while the energy gaps decrease linearly and symmetrically from the outermost NCs to the center. The values $i = 0$ and $N + 1$ denote the p- and n-type materials, represented by the left and right boxes in Figure 1, respectively, where $E_{0,N+1} = E_{\rm Bulk}$. For convenience, we associate a size $d_0 = d_{N+1} = 200$ Å to those materials. The position of the ith NC in the system is $x_i = \sum_{j=1}^{i-1} 2R_j + R_i$, for $2 \leq i \leq N$, with $x_1 = R_1$, and the total length of the NC array, $L_{\rm NC} = 2\sum_{i=1}^{N} R_i$, becomes $L_{\rm NC} \approx 2.61\,\mu$m. We proceed by discussing the model Hamiltonian and the Monte Carlo rules.

3 Coulomb interaction and Monte Carlo simulation rules

In the model, hopping of carriers occurs between nearest-neighbor NCs, or between a box and its neighboring NC, and the corresponding hopping time is denoted as $\tau_{\rm hop}$. This hopping time actually describes a tunneling process across energy barriers separating nearby clusters. In order to take into account the effects of passivation present on our NCs (see e.g. [6]), we assume that hopping in our array is hindered with respect to that in porous-Si and use here a value of $\tau_{\rm hop}$ which is 100 times larger than the one used for modelling carrier hopping in p-Si (cf. [10]). Thus, we take $\tau_{\rm hop} = 5 \times 10^{-3}$ s.

Electrons and holes, which are free to move in the doped materials, are pushed into the system (Fig. 1) by the applied electric field, $\vec{F}$, whose intensity is

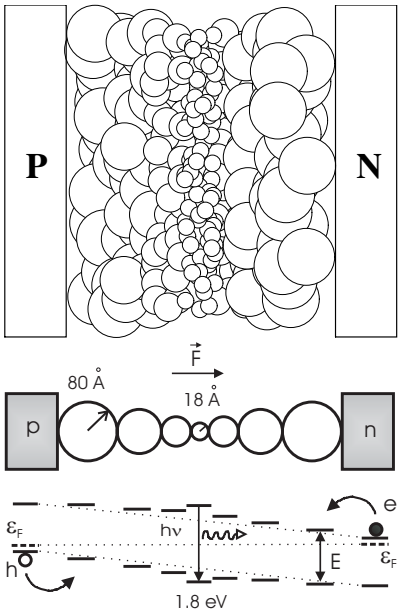

Fig. 1. Top panel: Illustration of an array of Si nanoclusters (open disks) of varying size (larger near the borders and smaller at the center of the array) sandwiched between p- and n-type doped silicon crystals (boxes), denoted by P and N. Lower panel: Schematic representation of the one-dimensional prototype model studied in this work. The energy levels (or optical gaps) of the neutral nanoclusters, in the absence of an external field, are illustrated at the bottom of the figure. In the stationary state, most of the photons (of ≈ 1.8 eV) will be emitted from the center of the system. The Fermi energy of the array, $\varepsilon_{\rm F}$, is indicated by the horizontal dotted line. The uppermost arrow indicates the direction of the applied electric field, $\vec{F}$, pointing in the forward bias direction to bring electrons e (small filled circle) and holes h (small open circle) from the borders to the center of the system. The additional dotted lines are drawn to guide the eye.

$F = U/L_{\rm NC}$, where U is the voltage drop and $L_{\rm NC}$ the total length of the array. In addition to the external field, the charge carriers react to the internal electric fields produced by the distribution of carriers inside the array. In order to move towards the center, electrons and holes have to overcome local energy barriers represented by the different energy gaps between neighboring NCs, undergoing thermally activated processes. It is further assumed that the external electric field does not modify the electronic structure of the NC.

To treat the carrier-carrier interactions consistently, the dielectric properties of the array must be considered. In order to simplify our approach, we take an effective dielectric constant $\varepsilon_{\rm eff}$ which is independent of position in the system (see e.g. [11,12]). Thus, the effective direct Coulomb interaction between the net charges q_i at x_i and q_j at x_j is given by

$$V_{i,j} = \frac{q_i q_j}{\varepsilon_{\rm eff}|x_i - x_j|} \quad , \qquad \text{for} \quad i \neq j \quad , \tag{1}$$

where $q_i = e(n_{\rm h}(i) - n_{\rm e}(i))$, and $n_{\rm h}(i)$, $n_{\rm e}(i)$ are the occupation numbers of h and e at the ith NC ($1 \leq i \leq N$), and

$e > 0$ is the unit electric charge. Due to charge neutrality, the net charges inside the doped materials are zero. Inside a single NC, the self-interaction of charges is estimated as (see also [11])

$$V_{i,i} = \frac{q_i^2}{\varepsilon_{\rm eff} R_i}. \tag{2}$$

Additional contributions due to exchange-correlation effects are not explicitly included in the model. They could be considered within a local density approximation as a correction to equation (2) (see e.g. [13]). Here, we take $\varepsilon_{\rm eff} = 2$ which is close to the value of the dielectric constant in p-Si [14]. Such a value is also consistent with estimates obtained from reference [11].

In order to study the transport of charges along the array we employ the Metropolis Monte Carlo (MC) algorithm which requires the calculation of the total energy of the system. The latter is evaluated according to the following semi-classical Hamiltonian,

$$\begin{aligned} E_{\rm tot}(\{n_{\rm e}, n_{\rm h}\}) = \sum_{i=1}^{N} \Bigg[& \left(\frac{E_i}{2} + \frac{E_{\rm Bulk}}{2L_{\rm NC}} \left(L_{\rm NC} - 2x_i \right) \right) n_{\rm e}(i) \\ & + \left(\frac{E_i}{2} + \frac{E_{\rm Bulk}}{2L_{\rm NC}} \left(2x_i - L_{\rm NC} \right) \right) n_{\rm h}(i) \Bigg] \\ & + E_{\rm Bulk}[n_{\rm e}(0) + n_{\rm h}(N+1)] \\ & + \sum_{i=1}^{N} \sum_{j=i}^{N} V_{i,j} - \sum_{i=1}^{N} F x_i q_i \\ & - eU[n_{\rm h}(N+1) - n_{\rm e}(N+1)], \end{aligned} \tag{3}$$

where the first two terms (those involving $E_{\rm Bulk}$) account for the energy of the particles occupying site i with respect to the Fermi level (see lower panel in Fig. 1), the third term represents the total Coulomb interaction, and the last two terms the potential energy of carriers due to the external field. The first two terms include the carrier energy due to the bandgap of the cluster at x_i and the contribution of the contact potential due to the n- and p-type semiconductors. We have assumed that the Fermi energy $\varepsilon_{\rm F}$ is coincident with the top of the valence band for the p-type semiconductor and coincident with the bottom of the conduction band for the n-type semiconductor (see bottom of Fig. 1). See Appendix B for more details.

In order to study the effects of the Coulomb interaction using Eq. (3), we consider the following three different models:

Model A: Full Coulomb interactions, with $V_{i,j} \neq 0$ for all i, j.

Model B: No Coulomb interactions, with $V_{i,j} = 0$ for all i, j.

Model C: Only local Coulomb (self-)interactions, where the local terms $V_{i,i} > 0$ for all $i = j$, and non-local ones $V_{i,j} = 0$ for all $i \neq j$.

In the next section we present results obtained from the three models in their steady state regimes, which are reached after about $10^5 N_{\rm tot}$ MC steps, and averages are performed over $5 \times 10^5 N_{\rm tot}$ MC steps.

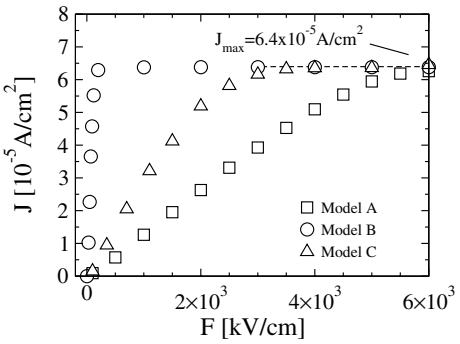

Fig. 2. Current density J versus applied electric field F. The maximum value $J_{\rm max}$ is obtained when the $n_{\rm h}(0) = \overline{n}$ holes and the $n_{\rm e}(N+1) = \overline{n}$ electrons hop in the time $\tau_{\rm hop}$ from the p- and n-boxes to the array, respectively. In these calculations, we have taken $\overline{n} = 8$.

4 Results and discussions

4.1 Models A, B and C: General behavior

Results for the current density J as a function of the electric field F are shown in Figure 2 for models A, B and C. In the limit $F \to \infty$, all the free carriers $n_{\rm h}(0)$ (in the p-box) and $n_{\rm e}(N+1)$ (in the n-box), jump to the array in a time $\tau_{\rm hop}$. Then, the maximum current density value $J_{\rm max} = e n_{\rm h}(0) / \left(d_0^2 \tau_{\rm hop} \right) = 6.4 \times 10^{-5}$ A/cm^2 is reached. From Figure 2 one can see that this asymptotic value is attained in each model for quite different values of F.

The resulting values for the current density J without interactions (model B) differ considerably from those with interactions (models A and C), while differing much less between those of models A and C. Regarding the experimentally accessible field intensities $F < 800$ kV/cm, we find for instance for $F = 100$ kV/cm, $J = 49.4 \times 10^{-6}$ A/cm^2 (model B) and $J = 0.92 \times 10^{-6}$ A/cm^2 (model A), i.e. the ratio between them is larger than one order of magnitude. Similarly, for $F = 500$ kV/cm we obtain $J = 63.8 \times 10^{-6}$ A/cm^2 (model B) and $J = 5.7 \times 10^{-6}$ A/cm^2 (model A). Thus, the Coulomb interaction reduces the current by an order of magnitude with respect to the case of no interaction. On the other hand, the ratio of current densities $J(F)$ from model C to those from model A is only of about 3 for fields ranging from 100 kV/cm to 800 kV/cm. This difference can be reduced by adjusting the value of $\varepsilon_{\rm eff}$ in model C. This point will be discussed in Section 4.4 below.

Another strong difference between the behavior of models A and C on one side, and those of model B on the other is the relation between J and the number $\overline{n}$ of holes and electrons in the p- and n-boxes. For a given value of F, J is directly proportional to $\overline{n}$ for model B. In contrast, for models A and C the current density J (and therefore also the total emission power) is rather insensitive to $\overline{n}$ (see top panel in Tab. 1).

This different behavior is mainly due to Coulomb self-interactions (see Eq. (2)) that limit the net charge in each nanocluster and thus the injection of carriers into the nanocluster array. Let us consider, as an example, the jump

Table 1. The values of the current density J and the mean maximum occupation number of electrons, $n_{\rm emax}$, and holes, $n_{\rm hmax}$, for models A, B and C in the case $F = 300$ kV/cm, for four different values of $\overline{n}$. For model B, the reported values have been obtained using the iterative method described in Section 4.3, whose error bars are much smaller than the ones obtained from the MC simulations. The numerical values for $n_{\rm emax}$ and $n_{\rm hmax}$ are equal within the statistical uncertainty.

	$J[10^{-5}$A/m]		
$\overline{n}$	Model A	Model B	Model C
1	0.20 ± 0.01	0.80	0.40 ± 0.02
8	0.30 ± 0.01	6.37	0.76 ± 0.02
64	0.39 ± 0.01	50.98	1.04 ± 0.02
512	0.40 ± 0.01	407.83	1.36 ± 0.02
	$n_{\rm hmax}$, $n_{\rm emax}$		
$\overline{n}$	Model A	Model B	Model C
1	1.1 ± 0.2	1	$2,2 \pm 0.2$
8	1.2 ± 0.2	8	3.4 ± 0.2
64	1.4 ± 0.2	64	5.3 ± 0.2
512	2.2 ± 0.2	512	6.4 ± 0.2

of one hole from the p-box to the $i = 1$ NC. In this case q_1 changes from $q_1 \to q_1 + 1$. We note that the Coulomb self-interaction (see Eq. (2)) is present in the $i = 1$ quantum dot but not in the p-box, which represents a bulk silicon crystal. In addition, one has that $q_1 \geq 0$ because there are (effectively) no electrons at site $i = 1$. Then, in the calculation of $E^{(\rm after)} - E^{(\rm before)}$ (see Eqs. (3) and (9)) the term $\left[(q_1+1)^2 - q_1^2\right]/\varepsilon_{\rm eff} R_1$ arises, which is positive. This term reduces the jump probability with respect to the case of no interaction (model B). We have a similar situation for the injection of electrons from the n-box to the $i = N$ quantum dot.

On the other hand, the combined effect of Coulomb self-interactions and recombinations limit the occupation number of electrons and holes in each nanocluster. For $F = 300$ kV/cm, the mean maximum number of holes, $n_{\rm hmax}$, and electrons, $n_{\rm emax}$, (with $n_{\rm hmax} = n_{\rm emax}$ by symmetry) in the array are shown in Table 1 for the three models. For model B one obtains $n_{\rm hmax} = \overline{n}$, and the occupation number can grow arbitrarily large leading to unphysical results.

4.2 Model A for 100 kV/cm $\leq$ F $\leq$ 800 kV/cm

The behavior of J as a function of F is shown in Figure 3 for model A in the range 100 kV/cm $\leq F \leq$ 800 kV/cm. A non monotonous increase of J is observed for increasing F. In particular, a small dip of J occurs around $F = 250$ kV/cm.

The dip observed for J in Figure 3 around $F = 250$ kV/cm is due to Coulomb interactions. Indeed, we have verified that such an 'undulating' behavior of the current with the applied field disappears when Coulomb interactions are switched off. In this respect, it is also interesting to study the behavior of the occupation numbers along the array for the external fields in question. The resulting particle profiles corresponding to the above mentioned three values of F are shown in Figure 4. Also here a non linear behavior of the profiles as a function of F appears. Note that although the current density J changes very little in going from point 1 to point 2 (see Fig. 3), a strong change in the corresponding charge occupation profiles occurs (see Fig. 4).

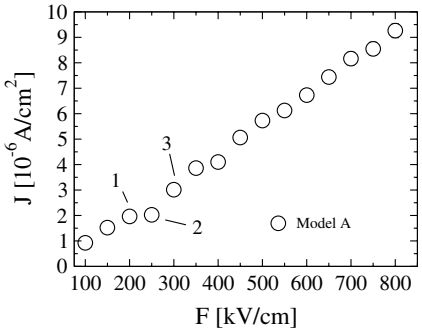

Fig. 3. Current density J versus applied electric field F for the full interactions model A. The points 1, 2 and 3 correspond to $F = 200$, 250, and 300 kV/cm, respectively. The actual error bars associated to J are smaller than the size of the symbols plotted in the figure.

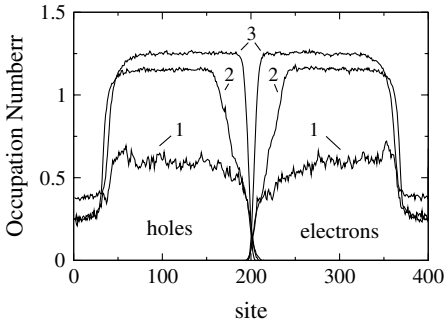

Fig. 4. The site occupation numbers $n_{\rm h}(i)$ and $n_{\rm e}(i)$ for model A for three values of F obtained using MC simulations. The curves 1, 2, and 3 correspond to $F = 200$, 250, and 300 kV/cm, respectively (see also Fig. 3).

In the steady state, all the electrons and holes that enter into the array get annihilated producing either photons or phonons, and J is proportional to the total recombination rate. As all recombinations effectively take place (in the stationary state) near the center of the array, we conclude that the shape of the occupation number profiles near the center is crucial for the determination of J. The detailed analysis of these features is beyond the scope of the present work. However, when the Coulomb interaction is suppressed (model B) J increases smoothly with F. Furthermore, as we discuss in what follows, a simple procedure can be implemented in this case by performing simplifying assumptions regarding the shape of the profile around the array center.

4.3 Model B: Analytical iterative procedure

Let us consider next the simplest transport model, i.e. the one in which Coulomb interactions are not present (model B). Monte Carlo results for the occupation numbers of electrons and holes are shown in Figure 5 for model B.

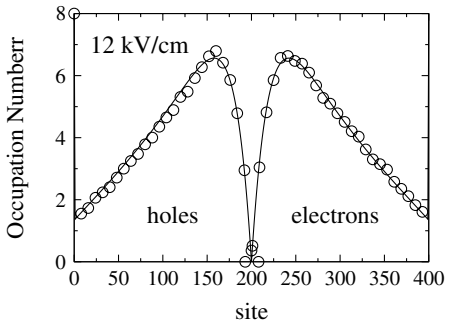

Fig. 5. The site occupation numbers for $F = 12$ kV/cm. The symbols correspond to results obtained from MC simulations without interactions (model B) and the lines represent the results of the iterative method, equations (4) and (5).

We can clearly observe that the charge distributions are well separated into two regions and that the number of electrons and holes tend to vanish near the center of the array, features common to the three models. Although small, the charge densities at the center are not identically zero, otherwise there would be no light emission from the array. The point is that annihilation of e-h pairs actually occurs on much shorter time scales than hopping, so that on average, the occupation numbers remain quite small in those sites where annihilation takes place. One can estimate values of occupation numbers at the center of the array in a simple way (see Appendix C).

For model B, the jump probabilities between nearest-neighbor sites do not depend on the charge distribution in the array. In this case it is possible to obtain the charge distribution (and also the current) using a simple iterative method.

In the analytical method we assume that holes are only present from site $i = 0$ to site $i = 200$, reflecting their behavior in the stationary state. This also means that electrons are only present in the right-half side of the array, i.e. $n_e(i) = 0$ for $0 \leq i \leq 200$. Clearly, in this simple approximation the two charge population do not overlap, implying that on average no e-h pairs are present at the center. This is not in contradiction with the fact that the device can still emit light, since both populations vanish (i.e. the charge carriers get annihilated) at the center of the array. Light emission can then be calculated from the resulting current in the array (see e.g. Appendix C).

From equations (3) and (9) one can compute the jump probabilities $p_{i,i+1}$ and $p_{i+1,i}$, with $0 \leq i \leq 200$. The same applies to electrons on the second half of the array. Then, the jump frequencies are given by $P_{i,i+1} = p_{i,i+1}/\tau_0$ and $P_{i+1,i} = p_{i+1,i}/\tau_0$, respectively. Let now $m_i(t)$ be the number of holes at site i at time t. The particle current in going from site i to site $i+1$ at time t is given by,

$$j_{i,i+1}(t) = m_i(t)P_{i,i+1} - m_{i+1}(t)P_{i+1,i}, \qquad (4)$$

and taking all these currents into account, one has that at time $t + \Delta t$,

$$m_i(t + \Delta t) = m_i(t) + [j_{i-1,i}(t) - j_{i,i+1}(t)]\,\Delta t, \qquad (5)$$

for $1 \leq i \leq 200$. The method consists in iterating equations (4) and (5) until a stationary (time independent) solution is reached. Here, we use the initial condition $m_i(0) = 0$ for $1 \leq i \leq 200$, with the boundary conditions $m_0(t) = 8$ and $m_{201}(t) = 0$ for all times t. The degree of convergence can be controlled by calculating the difference between two consecutive profiles as, $\epsilon^2(t + \Delta t) = \sum_i [m_i(t + \Delta t) - m_i(t)]^2/(200\Delta t)^2$. The iterations are stopped at time t_s when $\epsilon(t_s)$ becomes smaller than a predetermined threshold, ϵ_0.

Upon convergence, the resulting values $m_i(t_s)$ are considered as the average hole occupation numbers $n_h(i)$ in the steady state. In the present case, the electron distribution does not need to be calculated due to the assumed symmetry of the array. In our calculations we have typically used $\Delta t = 2.5 \times 10^{-3}$ s and $\epsilon_0 = 10^{-15}$ s^{-1}. The electrical current is obtained as $I = e j_{i,i+1}(t_s)$, which is independent of the index i.

In Figure 5 we report the calculated charge profiles obtained with the iterative method. One can see that the latter are in very good agreement with the results of Monte Carlo simulations. The iterative method is much faster than Monte Carlo simulations, specially for large values of the electric field F, where the occupation numbers per site can be very large making the MC simulations quite time consuming due to the presence of a large number of particles in the system.

Unfortunately, the iterative method cannot be extended to the case where the interactions $V_{i,j}$ are present, because the jump probabilities depend on the occupation numbers. Indeed, in equation (4) $j_{i,i+1}(t)$, $m_i(t)$, and $m_{i+1}(t)$ are the mean values of particle current and occupation numbers. Thus, equation (4) corresponds to a mean field approximation which is only valid when $p_{i,i+1}$ and $p_{i+1,i}$ do not depend on the occupation numbers. Although in the presence of self-interactions an analytical model similar to the above one can not be implemented, there exists a rather simple way of making the results of model C to get closer to those of model A.

4.4 Model C: Effective dielectric constant

We note that the values of J for model C are larger than those of model A (see Fig. 2). In order to reduce them one can adjust the value of the dielectric constant, $\varepsilon_{\rm eff}$, entering the self-interaction terms in model C. For smaller values of $\varepsilon_{\rm eff}$, $V_{i,i}$ increases (see Eq. (2)), and the occupation numbers decrease producing a diminution in J.

Monte Carlo results for J versus F, obtained from model C with $\varepsilon_{\rm eff} = 0.8$, are compared to those from model A ($\varepsilon_{\rm eff} = 2$) in Figure 6. The agreement is quite satisfactory for all values of F, in particular in the low-field region (see inset in Fig. 6) corresponding to the experimentally accessible electric fields.

Let us consider finally the emission spectra of the array in the two above cases. These are shown in Figure 7 for two different values of F. One can see that the corresponding spectra are quite similar and the associated total emission powers, $P_{\rm ph}$, are indeed very close to each other.

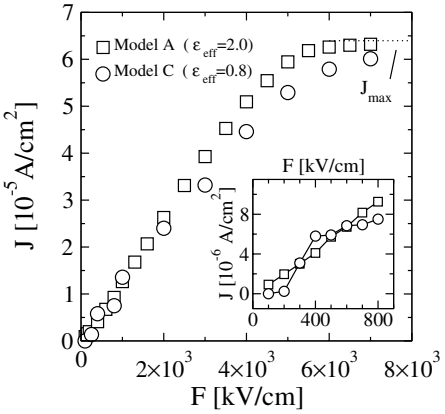

Fig. 6. Current density J versus applied electric field F for models A and C. The data were obtained using $\varepsilon_{\rm eff} = 2.0$ for model A and $\varepsilon_{\rm eff} = 0.8$ for model C (see Eqs. (1), (2), and (3)). The inset shows the same results but for F ranging from 100 to 800 kV/cm.

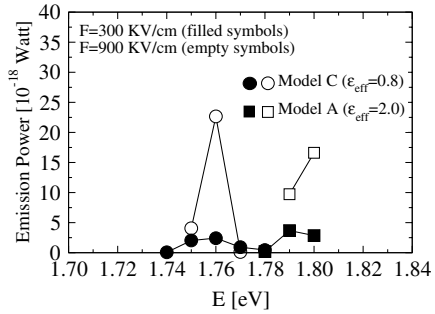

Fig. 7. Light emission spectrum of the NC array versus energy E for model A (squares) and model C with $\varepsilon_{\rm eff} = 0.8$ (circle). These results were obtained for two different values of F: $F = 300$ kV/cm (filled symbols), and $F = 900$ kV/cm (empty symbols). The total emission in each case is found to be: $P_{\rm ph} = 6.73 \times 10^{-18}$ W (filled squares), $P_{\rm ph} = 5.88 \times 10^{-18}$ W (filled circles), $P_{\rm ph} = 2.68 \times 10^{-17}$ W (empty squares) and $P_{\rm ph} = 2.63 \times 10^{-17}$ W (empty circles). Although the total emissions for the same value of F are similar, the spectra for model C are shifted to the red with respect to those from model A.

Monte Carlo simulations for model A require, however, a total computation time much larger than for model C. This is due to the terms $V_{i,j}$ with $i \neq j$, corresponding to long range interactions. A quantitative comparison between both models indicate that the effects of such long-range interactions can be approximately taken into account by using an appropriate dielectric constant. Numerically, the advantage of using model C instead of the full interactions model A, resides in the saving of computational effort. This fact can become very useful in the study of more complex nanocluster arrays, in particular for higher-dimensional versions of the model as the one shown in the top panel of Figure 1.

5 Conclusions

In conclusion, carrier-carrier interactions must be taken into account in realistic simulations of charge transport in silicon nanocluster arrays. Differently from the case of bulk semiconductors, silicon nanoclusters are distinct materials due to both quantum-confinement effects and the presence of non-vanishing Coulomb interactions among charge carriers. Both features lead to a characteristic behavior of transport in such nanoscales. In particular, silicon nanoclusters, although displaying efficient light emission properties, have rather poor conducting behavior when constituting optoelectric devices, since the presence of intra-cluster Coulomb interactions alone (in addition to passivation effects) limits the electron-hole recombination currents yielding low emission powers. Nonetheless, the present study sheds some light into the quantitative aspects of transport in silicon-based nanoarrays, indicating a way of performing suitable approximations with the hope of being able to design, and therefore simulate complex, new useful structures. The main result of the work indicates that Coulomb interactions do not need to be taken fully into account, rather, a simpler interaction model with intra-clusters (i.e. local) interactions is sufficient to achieve semi-quantitative results.

Appendix A: The model of silicon nanoclusters

In intrinsic silicon nanoclusters the optical gap E between electron and hole energies depends on NC size. Specifically, the relation between E (in eV) and the radius R of a nanocluster is given by [6]

$$R(E) = \frac{13\,({\rm eV})^{0.72}}{(E - E_{\rm Bulk})^{0.72}}\ \text{Å}, \tag{6}$$

where $E_{\rm Bulk} = 1.17$ eV is the indirect optical gap of bulk silicon. We assume that the electron-hole recombinations take place when both the electron and the hole are present inside the same nanocluster. The recombination can be radiative (producing a photon) or non-radiative (producing a phonon). For E in the range $1.2\ {\rm eV} < E < 2$ eV, and at a temperature $T = 300$ K, one can obtain from [10] the following radiative recombination time

$$\tau_{\rm rad}(E) = \frac{7.7 \times 10^{-4}\,({\rm eV})^{1.38}}{(E - E_{\rm rad})^{1.38}}\ {\rm s}, \tag{7}$$

where $E_{\rm rad} = 1.137$ eV. From [6] the non-radiative recombination time, $\tau_{\rm nrad}(E)$ can be estimated (see e.g. [9]) as

$$\tau_{\rm nrad}(E) = \frac{Y(R)}{1 - Y(R)}\tau_{\rm rad}(E), \tag{8}$$

where the photoluminescence yield $Y(E) \equiv \tau_{\rm nrad}/(\tau_{\rm rad} + \tau_{\rm nrad})$, behaves as $Y(E) = 4.4\exp(-2R/14\ \text{Å})$, for $R \geq 18$ Å. From equations (6)-(8) and for a given value of gap E, one obtains the radius R of the nanocluster and its radiative and non-radiative recombination times, $\tau_{\rm rad}$ and $\tau_{\rm nrad}$. For example, for $E = 1.25$ eV ($R \approx 80$ Å), $\tau_{\rm rad} \approx 1428\ \tau_{\rm nrad} = 1.6 \times 10^{-2}$ s, while for $E = 1.8$ eV ($R = 18$ Å), both recombination times are of comparable magnitude, $\tau_{\rm rad} \approx 2\tau_{\rm nrad} = 1.4 \times 10^{-3}$ s, i.e. radiative recombinations are relatively more efficient at smaller radii R than at large ones. This is the reason why the nanoclusters of about 18 Å of radius are located at the center of the array (see Fig. 1) where the emission of light occurs.

Appendix B: Monte Carlo rules

To implement the MC simulations, we consider the total number of electrons $N_{\rm e} = \sum_{i=0}^{N+1} n_{\rm e}(i)$, holes $N_{\rm h} = \sum_{i=0}^{N+1} n_{\rm h}(i)$, and e-h pairs $N_{\rm p}$ defined as $N_{\rm p} = \sum_{i=1}^{N} n_{\rm p}(i)$, where $n_{\rm p}(i) = \min(n_{\rm e}(i), n_{\rm h}(i))$ (for instance, if $n_{\rm e}(i) = 2$ and $n_{\rm h}(i) = 3$, then $n_{\rm p}(i) = 2$). Then, at each MC step, we chose one of these $N_{\rm tot} = N_{\rm e} + N_{\rm h} + N_{\rm p}$ elements at random.

If a particle (electron or hole) is selected, say at site i, it can either hop to one of the two neighboring sites or remain at i. A hop occurs with a probability

$$p_{i\to j} = p_{\rm hop}\,\exp(-\beta \Delta E_{\rm tot}), \quad \text{for} \quad \Delta E_{\rm tot} > 0, \quad \text{and}$$
$$p_{i\to j} = p_{\rm hop}, \quad \text{otherwise}, \tag{9}$$

where $p_{\rm hop} = \tau_0/\tau_{\rm hop}$, τ_0 is the time unit, $\Delta E_{\rm tot} = E_{\rm tot}^{\rm (after)} - E_{\rm tot}^{\rm (before)}$ the variation of the total energy of the system for the attempted jump from site i to j, and $\beta = 1/K_{\rm B}T$. Here we use $T = 300$ K. Hops from site $i = 0$ can only occur to site $i = 1$, and from site $N + 1$ to site N. When a hopping process involves the left or right box, the particle occupation inside the box is restored to its predetermined value immediately after the hop has occurred. For the case of equally doped p- and n-material, the number of carriers in the boxes is taken as $n_{\rm h}(0) = n_{\rm e}(N + 1) = \overline{n}$. In the present calculations we have taken $\overline{n} = 8$, yielding a density of free carriers $\overline{\rho} = \overline{n}/d_0^3 = 1 \times 10^{18}$ cm^{-3} inside both doped materials.

In the case a pair is selected, a recombination event, either radiative or non-radiative, takes place with probabilities $p_{\rm rad} = \tau_0/\tau_{\rm rad}$ and $p_{\rm nrad} = \tau_0/\tau_{\rm nrad}$, respectively. Here, we have used $\tau_0 = 5 \times 10^{-5}$ s, and at each MC step the time is increased by $\Delta t = \tau_0/N_{\rm tot}$.

In our practical calculations we do not simulate the motion of carriers inside the doped materials, which are assumed to be just the sources of charges entering the array. Instead, we set a potential drop U across the NC array of length $L_{\rm NC}$ and introduce a number of holes, $\delta n_{\rm h}(0)$, and electrons, $\delta n_{\rm e}(N + 1)$, at sites 0 and $N + 1$ at each MC step, respectively, to keep the mean density of carriers inside the doped materials at their values, $\overline{\rho}$. The current is then given by the mean number of electrons and holes that enter the system per unit time, $I = e\langle \delta n_{\rm h}(0) + \delta n_{\rm e}(N + 1)\rangle/\Delta t$, while the associated current density, J, is estimated as $J = I/d_0^2$. Finally, the total emission power, $P_{\rm ph}$, is given by $P_{\rm ph} = \sum_{i=1}^{N} N_{\rm ph}(i)\, E_i$, where $N_{\rm ph}(i)$ is the mean number of radiative recombinations per unit time at site i.

Appendix C: Occupation numbers at the center of the array

We can estimate in a simple way the number of e-h pairs, $n_{\rm p}$, at the center of the array by assuming that all the charges entering the system per unit of time get annihilated at the central sites. Thus, the current I can be estimated as $I = e n_{\rm p}/\tau_{\rm rec}$, where the total recombination time

$$\frac{1}{\tau_{\rm rec}} = \frac{1}{\tau_{\rm rad}} + \frac{1}{\tau_{\rm nrad}} \approx \frac{1}{0.47\ {\rm ms}}, \tag{10}$$

since $\tau_{\rm rad} = 2\tau_{\rm nrad} = 1.4$ ms for a NC of radius $R = 18$ Å (see end of Appendix A). Since by definition, the current density $J = I/d_0^2$, we have

$$n_{\rm p} = \tau_{\rm rec}\frac{J}{e} d_0^2. \tag{11}$$

Using the results from model A for $F = 250$ kV/cm, where $J = 2.067 \times 10^{-6}$ A/cm^2 (see Fig. 3), we get $n_{\rm p} \approx 0.024$, which is a small number. If in equation (11) we use the maximum possible current in the device, $J_{\rm max}$ (see Sect. 4.1), we obtain

$$n_{\rm p} = n_{\rm h}(0)\frac{\tau_{\rm rec}}{\tau_{\rm hop}}, \tag{12}$$

which depends on the ratio between the two characteristic times in the problem. In the case $n_{\rm h}(0) = 8$ we find $n_{\rm p} = 0.752$. This number can be compared to the average occupation number obtained in the case of large fields. For instance, in the case $F = 6000$ kV/cm, the later is about $8 \gg n_{\rm p}$.

This work is partially supported by the MAE (Italy) and the SETCIP (Argentina) through the Scientific Collaboration Program between Italy and Argentina (project Nr. 31, Ref. 22F). K.I.M. and H.O.M. also acknowledge partial financial support from the CONICET (Argentina) and ANPCyT (Grant Nr. 03-08431, Argentina).

References

1. L.T. Canham, Appl. Phys. Lett. **57**, 1046 (1990)
2. L. Pavesi, J. Phys.: Condens. Matter **15**, 1169 (2003)
3. M.H. Nayfeh, S. Rao, N. Barry, J. Therrien, G. Belomoin, A. Smith, S. Chaieb, Appl. Phys. Lett. **80**, 121 (2002)
4. A. Fujiwara, K. Yamazaki, Y. Takahashi, Appl. Phys. Lett. **80**, 4567 (2002)
5. M. Ben-Chorin, F. Möller, F. Koch, W. Schirmacher, M. Eberhard, Phys. Rev. B **51**, 2199 (1995)
6. G. Ledoux, J. Gong, F. Huisken, O. Guillois, C. Reynaud, Appl. Phys. Lett. **80**, 4834 (2002)
7. L. Pavesi, L. dal Negro, C. Mazzoleni, G. Franzó, F. Priolo, Nature **408**, 440 (2000)
8. L.T. Canham, Nature **408**, 411 (2000)
9. K.I. Mazzitello, H.O. Mártin, C.M. Aldao, H.E. Roman, J. Phys. D: Appl. Phys. **37**, 668 (2004)
10. H.E. Roman, L. Pavesi, J. Phys.: Condens. Matter **8**, 5161 (1996)
11. G. Allan, C. Delerue, M. Lannoo, E. Martin, Phys. Rev. B **52**, 11982 (1995)
12. R. Tsu, D. Babić, Appl. Phys. Lett. **64**, 1806 (1994)
13. R.A. Broglia, G. Coló, G. Onida, H.E. Roman, *Solid State Physics of Finite Systems: Metal Clusters, Fullerenes, Atomic Wires* (Springer Verlag, Berlin, 2004)
14. I. Sagnes, A. Halimaoui, G. Vincent, P.A. Badoz, Appl. Phys. Lett. **62**, 1155 (1993)